Soil textural classification by a photosedimentation method

Paul K. Buah-Bassuah, Stefano Euzzor, Franco Francini, Gabriel W. Quansah, and Paola Sansoni

A photosedimentation technique is used to analyze the size composition of soil samples. The number and size of the particles are determined, respectively, by the Stokes formula and the Beer–Lambert law, measuring time-of-flight and laser light attenuation simultaneously and hence evaluating solution turbidity. A simple software procedure has been developed to obtain fractional volume size distribution, taking into account the particle's optical properties depending mainly on its size and refractive index. Laboratory measurements on calibrated particulates, showing their reproducibility and validation as well as a classification of ground samples, are presented. Size distribution data can then be utilized to obtain a textural classification of the soil samples for agricultural applications.

OCIS codes: 350.4990, 290.0290, 290.2200.

1. Introduction

The physical properties of powdery samples such as soil and clay for various applications in the pharmaceutical, paint-pigment, cement, ore flotation, photographic-emulsion, and ceramic industries are related to knowledge of the size distribution of the grains that constitute the powder.[1] To measure the fineness of the grains of these powdery samples and other powder–fluid systems, one has to assess the suitability of the method required to accomplish such size analysis. For example, microscopic examination of particles gives direct information on particle shape and particle diameter ($2r$) from a few millimeters to 1 μm. Sieve analysis, on the other hand, allows measurements of particle sizes from 5 μm upward.[1] The limitation of these methods is based mostly on operator errors. The sedimentation technique, which relies on concentration changes that occur within a settling suspension of the powder, is based on the Stokes formula for determination of the size distribution of particles that range between $r =$ 1 μm and a few hundred micrometers, provided that the density of the powder is sufficiently different from that of the liquid.

For the sedimentation method, pipette, hydrometer, and specific gravity balance[1] are the common apparatuses used. However, both apparatuses are in contact with the sample in suspension and they can disturb the solid content of the initial suspension. In low concentration cases,[2] the use of the hydrometer for measurement of the particle sizes does not guarantee reliable results.

The sedimentation technique, with the use of a light source to obtain light extinction (scattering and absorption) by the sedimenting particles under free fall, improves the measurement procedure since it is a noncontact technique that deals with samples in small quantities. The size of the particles is determined from the signals corresponding to the intensity of the transmitted light. For the study of sedimentation of powdery substances, it is useful to consider the time of flight that can be measured with a laser beam. Monitoring the particle velocities in dilute suspension offers a reliable and time-saving technique for measuring size distribution.[3]

We present a method to determine the size distribution of powdery samples, such as aluminum oxide particles, and soil samples by laboratory measurements based on a photosedimentation technique that uses laser light extinction. The particles should be homogeneously dispersed in the solution and their sedimentation that is due to gravity is measured by an incremental procedure.

P. K. Buah-Bassuah and G. W. Quansah are with the Department of Physics, University of Cape Coast, Cape Coast, Ghana; S. Euzzor, F. Francini, and P. Sansoni are with the Istituto Nazionale di Ottica, Firenze 50125, Italy.

Received 3 September 1997.
0003-6935/98/030586-08$10.00/0

2. Theory

Let us consider a statistically homogeneous dispersion of identical rigid spherical particles of radius r and density ρ_s in a Newtonian ambient fluid of viscosity η and density ρ. If the spherical particle of weight w ($w = mg$, where m is the mass of the particle and g is the acceleration that is due to gravity) falls freely with velocity u through the fluid and is subjected to resultant force F_g that is due to gravitational and hydrostatic forces in the direction of motion, there is a viscous drag force F_v opposed to the motion.

The resultant force F_g can be expressed as

$$F_g = (4/3)\pi r^3(\rho_s - \rho)g, \tag{1}$$

and the viscous drag force F_v is given by the Stokes equation

$$F_v = 6\pi\eta u r. \tag{2}$$

When $F_v = F_g$, the particle falls with a constant or terminal velocity (sedimentation velocity) u_o whose value is given by

$$u_o = \frac{2}{9}\frac{(\rho_s - \rho)g}{\eta}r^2. \tag{3}$$

Considering a suspension of spheres at a volume concentration ϕ, we can observe that the velocity of sedimentation of the particles is controlled by the upward motion of the fluid, and the magnitude of the terminal velocity is expressed as[4]

$$u = u_o(1 - k\phi), \tag{4}$$

where k is a constant whose theoretical value is 6.55 and ϕ is the volume concentration. Velocity u of a particular sphere differs from u_o owing to the hydrodynamic interaction between the various particles in the dispersion, and $u - u_o$ is a random quantity with a nonzero mean value that depends on the volume concentration of the particles. If the volume concentration is of the order of 10^{-3}, the difference between the terminal velocity and the value corresponding to the infinite solution is less than 1%. By substituting Eq. (3) into Eq. (4), we obtain an expression for the terminal velocity. The size distribution can then be determined from the distribution of sedimentation velocities at low volume concentrations.

The measurement of sedimentation velocities of particles is derived from the intensity of the light transmitted through a scattering cell filled with a suspension of particles. If I_o is the incident light intensity and I is the intensity transmitted beyond the cell, the light attenuation that is due to the particles is expressed by the Lambert–Beer law

$$(I/I_o) = \exp(-\gamma d), \tag{5}$$

where d is the cell thickness (in the optical axis direction).

This exponential attenuation is due to two different effects, scattering and absorption, and their sum is represented by the extinction coefficient γ, defined as

$$\gamma = \pi r^2 N Q_{\text{ext}}, \tag{6}$$

where r is the radius of the sphere, N is the number of particles in the unitary volume, and Q_{ext} is the extinction efficiency. As shown in Section 4, Q_{ext} is strongly dependent on the particle radius for small values ($r < 5$ μm), whereas for higher r values Q_{ext} tends to a value of 2. Furthermore Eq. (5) can be expressed as

$$\ln(I/I_o) = \pi r^2 N Q_{\text{ext}} d. \tag{7}$$

On the other hand, from Eq. (3) we can obtain the radius of the particle, depending on particle time of flight t, as well as on the distance (h) between the liquid top surface and the position of the laser beam lamina cutting the cell, as follows:

$$r(t) = \left[\frac{9\eta h}{2(\rho_s - \rho)g}\right]^{1/2} t^{-1/2} = Zt^{-1/2}, \tag{8}$$

where

$$Z = \left[\frac{9}{2}\frac{\eta h}{(\rho_s - \rho)g}\right]^{1/2} \tag{9}$$

is a constant that depends on the spheres (ρ_s) and liquid (ρ) densities, on the viscosity (η), and on the height (h); the constant ratio 9/2 denotes a geometric factor derived from the spherical shape of the particle.

The number of particles corresponding to each size value present in the scattering cell can then be derived from Eqs. (7) and (8). For each value I_k (with $k = 1, \ldots, n$) of the intensity measured through the solution at time t_k, corresponding to size r_k, we can rewrite Eq. (7) to generate system 1:

$$\begin{aligned}
\ln(I_1/I_o) &= d\pi(N_1Q_1{r_1}^2 + N_2Q_2{r_2}^2 + \ldots + N_nQ_n{r_n}^2),\\
\ln(I_2/I_o) &= d\pi(N_1Q_1{r_1}^2 + N_2Q_2{r_2}^2\\
&\quad + \ldots + N_{n-1}Q_{n-1}{r_{n-1}}^2),\\
\ln(I_3/I_o) &= d\pi(N_1Q_1{r_1}^2 + N_2Q_2{r_2}^2\\
&\quad + \ldots + N_{n-2}Q_{n-2}{r_{n-2}}^2),\\
\ln(I_k/I_o) &= d\pi(N_1Q_1{r_1}^2 + N_2Q_2{r_2}^2\\
&\quad + \ldots + N_{n-k+1}Q_{n-k+1}{r_{n-k+1}}^2),\\
\ln(I_n/I_o) &= d\pi(N_1Q_1{r_1}^2), \qquad \text{(system 1)}
\end{aligned}$$

where N_k represents the number of particles in the class of dimensions r_k (for $k = 1, \ldots, n$), and the corresponding extinction efficiency $Q_{\text{ext}k}$ is indicated by the simplified notation Q_k.

Substituting Eq. (8) into Eq. (7), we finally obtain Eq. (10) relating the transmitted laser light, derived from the falling of the different masses or sizes of

particles, to the settling time t of the sedimenting particles:

$$\ln(I/I_o) = \pi N Q_{\text{ext}} d Z^2 (1/t). \tag{10}$$

Thus defining $\ln(I_k/I_o)/(Z^2\pi d) = L_k$ (for each $k = 1, \ldots, n$), where d is the thickness of the scattering cell, system 1 becomes

$$\begin{aligned}
L_1 &= (N_1Q_1/{t_1}^2 + N_2Q_2/{t_2}^2 + \ldots + N_nQ_n/{t_n}^2)\\
L_2 &= (N_1Q_1/{t_1}^2 + N_2Q_2/{t_2}^2 + \ldots + N_{n-1}Q_{n-1}/{t_{n-1}}^2)\\
L_3 &= (N_1Q_1/{t_1}^2 + N_2Q_2/{t_2}^2 + \ldots + N_{n-2}Q_{n-2}/{t_{n-2}}^2)\\
L_k &= (N_1Q_1/{t_1}^2 + N_2Q_2/{t_2}^2\\
&\quad + \ldots + N_{n-k+1}Q_{n-k+1}/{t_{n-k+1}}^2)\\
L_n &= (N_1Q_1/{t_1}^2) \qquad \text{(system 2)}
\end{aligned}$$

The extinction efficiency values Q_1, $Q_2, \ldots, Q_k, \ldots Q_n$ pertain to each dimension class and can be evaluated by the following expression derived from the Mie theory for spherical particles:

$$Q_k = Q_{\text{ext}k} = \frac{C_{\text{ext}k}}{\pi {r_k}^2} = \sum_{j=1}^{\infty} (2/{\alpha_k}^2)(2j+1)\text{Re}(a_j + b_j). \tag{11}$$

Q_k is the extinction efficiency corresponding to the scattering cross section $C_{\text{ext}k}$ obtained from the scattering coefficients of the Mie theory[5,6] a_k and b_k. Each calculation was performed for a monodispersed distribution with radius r_k and a size parameter defined as $\alpha_k = 2\pi r_k/\lambda$ for the radiation wavelength λ, for each $k = 1, \ldots, n$.

The Q_{ext} values can be obtained, considering the particles as spheres, by the Mie theory by use of a program based on the Bohren–Huffman–Mie routine presented in Ref. 7. For this calculation one must know the real and imaginary parts of the refractive index, together with the wavelength and size distributions of the particles.

With this procedure system 2 can be easily solved, which allows us to obtain the values of the particle size distribution $N_1, N_2, \ldots N_k, \ldots N_n$. System 2 is composed of a series of equations that were obtained by dividing (by the factor $Z^2\pi d$) each equation of system 1. Therefore each L_k value is proportional to the logarithm of the intensity ratio I_k/I_o, and each value corresponds to the time value t_k ranging between t_1 and t_n. This set of time sampling values is derived by means of Eq. (8) from the radius sampling values, which represent the resolution of the final size distribution results given in Sections 5 and 7.

3. Experimental Procedure and Measurements

A 5-mW He–Ne laser beam at a wavelength of 0.633 μm was expanded by a beam expander (BE) and diaphragmed by a slit ($b = 1$ mm) to produce a thin horizontal beam lamina with a dimension corresponding to the 7 × 5-cm glass cell base (Fig. 1).

This beam lamina was incident on the plane lateral face of the cell, which measures 7 cm × 40 cm perpendicular to the beam axis. The cell was initially filled with distilled water, and its dimension in the beam direction (Fig. 1) is thickness $d = 5$ cm. The intensity of the light attenuated by water and falling particles was detected beyond the cell by a photodetector interfaced to a PC through an amplifier and an analog-to-digital (A/D) converter. The laser source, the glass cell with its contents, and the photodetector (PD) were optically aligned. Figure 1 shows some of the system's linear dimensions, including the typical range of values (3–10 cm) for height h between beam level and water surface level in the cell.

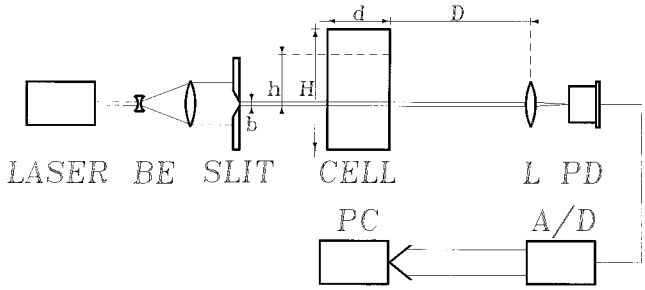

Fig. 1. Laboratory setup scheme distances: $b = 1$ mm, $H = 40$ cm, $d = 5$ cm, $D = 2$ m, and h lies between 3 and 10 cm.

For application of the Lambert–Beer law one must measure only the transmitted light, and this requires that the cell has plane lateral faces to avoid focusing the light with the cell. Furthermore to measure only the transmitted light without the scattering contribution, the light must be detected within a small (a few millirads) scattering angle. Since the scattering semiangle is defined as $\beta = R/D$, where D is the distance between the cell and the detector and $2R$ is the detector diameter, a detector with $2R = 1$ cm must be placed at approximately $D = 2$ m to obtain a sufficiently small scattering semiangle ($\beta = 2.5$ mrad). As an alternative to increasing distance D, obviously, it is possible to reduce the detection area, for example, by a diaphragm: to obtain the same $\beta = 2.5$ mrad with $D = 30$ cm, $2R$ should be 1.5 mm. Moreover lens L improves the detection by focusing all the light intensity of the 70 mm × 1 mm beam lamina into the detector area of diameter $2R = 1$ cm.

Some early experiments were performed with calibrated aluminum oxide particles dispersed in distilled water. Before beginning the data acquisition the cell was completely reversed to a downward position to have all the particles uniformly dispersed. The cell was then reversed to its original upright position to allow the particles to fall freely. As the particles fell and traversed the beam lamina, the transmitted intensity I and the corresponding time of flight t (in seconds) were immediately and simultaneously recorded on the computer and a graph of I versus t was automatically plotted. For each measurement the reference light intensity I_o (light transmitted through the cell with only distilled water) was recorded before we started the acquisition with the samples in the dispersive medium. Thus the I/I_o ratio can be evaluated as a function of time to obtain

the L_k values of system 2. The experiment was performed at a room temperature of 20 °C.

For the validation tests, three different sizes of calibrated aluminum oxide particulate were examined separately and then as mixtures of two or three different diameters. The method was then applied to the examination of two soil samples poured into a solution of distilled water and sodium pyrophosphate, added as a wetting agent. Size distribution results pertaining to the aluminum oxide particles and to the ground samples are shown in Sections 5 and 7, respectively.

4. Data Analysis

Two fundamental assumptions are required to apply the theory presented in Section 2 to the data elaboration of the size measurements described in Section 3. One is that the particles are considered as spheres for the calculation of their optical properties (extinction efficiencies and cross sections) with the Mie theory. The other is that the Stokes formula can be applied beyond its limiting value corresponding to $r \approx 30$ μm (using water solution) to as much as a few hundred micrometers.

The limiting values for the laminar flow region[1] in which the Stokes formula holds can be expressed by the Reynolds number Re, defined as

$$Re = \frac{(2r)^3(\rho_s - \rho)\rho g}{18\eta^2}.$$

Referring to the η and ρ values of water listed below and considering for ρ_s the typical values (of quartz and kaolin) reported in Section 6, the Stokes formula can be strictly applied up to $r = 30$ μm corresponding to $Re = 0.2$. Beyond this region of laminar flow there is an intermediate region and for $Re > 2000$–3000 the flow becomes turbulent. Our size measurements in water were carried out to a few hundred micrometers, corresponding to $Re < 100$. To measure higher size values it is necessary to use a fluid with higher density to decrease the Reynolds number and restore the laminar flow regime into the system.

In the laboratory the transmitted intensity versus time was measured and recorded in a data file as the first step of the measurement procedure. The extreme values of size range chosen for each measurement define its duration, depending on the minimum radius value ($r = 2$ μm), as well as the sampling time, determined by the maximum r value ($r = 300$ μm) to be measured. As the second step, the L_k values in system 2 were calculated by selecting the light intensity values I_k from among all those recorded (every 100 ms). The third step of the procedure consisted of data elaboration on the basis of the Stokes formula, Eq. (8), and the Lambert–Beer law, Eq. (5). The attenuation that is due to water absorption was taken into account by dividing the I_k values by the reference value I_o, which were recorded with the cell containing only water. Moreover, the Q_{ext} values corresponding to the sampling r values were evaluated, and the equations in system 2 were solved by subtraction beginning with the last equation. The final results for the fractional size distribution, normalized in volume, are presented in Sections 5–7.

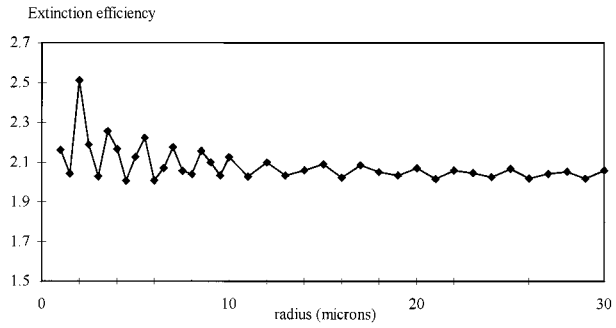

Fig. 2. Extinction efficiency $Q_{ext}(r)$ of aluminum oxide.

The parameters required for this calculation are: water density $\rho = 1000$ kg/m^3, water viscosity $\eta = 0.001$ nN, gravity acceleration $g = 9.81$ m/s^2, and the particle density (ρ_s) is 3560 kg/m^3 for aluminum oxide (Al_2O_3). Depending on these constants, the height (h) must be chosen to obtain a measurable time of flight for the extreme size values (see Tables 2–4).

The use of Eq. (9) in system 2 requires a detailed calculation of the extinction efficiency Q_{ext} values, with a sampling rate corresponding to the values chosen for the size analysis (i.e., the step between the maximum and minimum sizes). For this calculation, one must know both the real and imaginary parts of the relative refractive index $m = m_s/m_w$ (of the particle with respect to the surrounding medium, distilled water in this case $m_w = 1, 0$). Figure 2 gives the Q_{ext} values of aluminum oxide ($m_s = 1.77, 0$). For size values of 1-μm spacing, the corresponding Q_{ext} values have been obtained, taking into consideration monodispersed distributions and the He–Ne wavelength. In agreement with the Mie theory, the extinction efficiency values oscillate for small sizes and approach their theoretical limiting value of 2 as the size increases.

Since the chosen size range of our sedimentation measurement was between a few micrometers and a few hundred micrometers, the aluminum oxide particulates selected for the validation tests were size dispersed with an average radius $r = 3$, 14.5, and 25 μm.

The contribution that is due to Brownian motion in this size range can be considered negligible compared to gravitational settling. It has been calculated[1] that the displacement that is due to Brownian motion with respect to gravitational settling (in water at 21 °C) is 0.4% for $r = 10$ μm, 2.4% for $r = 2.5$ μm, and 134% for $r = 1$ μm. Therefore for radius values higher than 2 μm the Brownian motion need not be taken into account.

5. Reproducibility and Validation of the Measurements

The laboratory setup, measurement procedure, and computer elaboration were tested and optimized by some preliminary measurements on calibrated particles. These were aluminum oxide (Al_2O_3) particles,

Table 1. Measurements on Calibrated Samples

Measurement Number	Measured Radius (μm)	Height h (cm)	Measurement Duration (min)	Nominal Radius (μm)
mis 1	23 ± 2	3.2	2	25
mis 2	23 ± 2	2.6	2	25
mis 3	26 ± 1	3.0	2	25
mis 4	24 ± 2			25
	13 ± 2	3.0	4	14.5
mis 5	27 ± 1			25
	16 ± 2	2.8	4	14.5
mis 6	25 ± 1			25
	14 ± 2	2.8	60	14.5
	2.5 ± 1			3
mis 7	27 ± 1			25
	14 ± 1	2.95	60	14.5
	3 ± 0.5			3
mis 8	25 ± 2			25
	13 ± 2	10.0	160	14.5
	3.5 ± 1.5			3
mis 11	25 ± 1	3.0	2	25
mis 12	25 ± 2	2.9	2	25
mis 13	26 ± 1	3.0	2	25
mis 14	25 ± 1			25
	14 ± 1	2.8	4	14.5
mis 15	26 ± 1			25
	14 ± 2	3.2	4	14.5
mis 16	24 ± 2			25
	15 ± 1	2.8	60	14.5
	3.5 ± 1			3
mis 17	24 ± 1			25
	14 ± 1	2.8	60	14.5
	4 ± 1			3
mis 18	24 ± 1			25
	14 ± 1	9.0	160	14.5
	4.5 ± 1.5			3

typically used for optics (from Buehler, Ltd.), with nominal size distributions centered at three average values: r = 25.0, 14.5, and 3.0 μm.

Measurements on the same samples were repeated both to prove reproducibility of the procedure and to compare the results to validate the measurement and elaboration procedure. As Table 1 reports, measurements were first made by introducing particles with only r = 25 μm. We then added those with r = 14.5 μm and finally all three calibrated particulates were measured together. Results were preliminarily compared with other measurements on the same samples; then the mean radius of the measured size distribution was compared with the nominal radius indicated for the aluminum oxide particles by the supplier.

Table 1 summarizes the results of two groups of measurements performed on calibrated particulates indicating the duration and height h pertaining to each measurement. The validation of the measurement procedure is represented by the agreement between the measured radius values (second column) and those indicated by the supplier of the calibrated particles (last column).

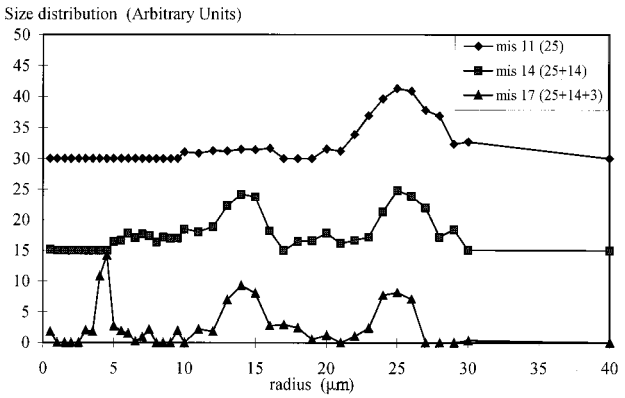

Fig. 3. Fractional volume size distribution of calibrated particles (r = 3.0, 14.5, 25.0 μm). Curves labeled as mis 11 and mis 14 are vertically shifted by 15 and 30 units, respectively, keeping the same x axis.

For the largest particles (r = 25.0 μm) measurements lasted 2 min, when we chose height h = 3 cm, whereas for r = 14.5 μm the measurement duration was 4 min for the same height h. The smallest particles (r = 3 μm) required 2 h 40 min of measurement time for h = 9 cm, but when we use higher h values, the experiment lasts several hours. Height h was chosen to have good sensitivity for the largest particles (h large enough for measuring the time of flight for the largest particles: a few fractions of a second) and an acceptable measurement duration (the time of flight for the smallest particles increasing with h) (see Tables 2–4).

Figure 3 presents an example of a series of three measurements that were performed: the first only with particles of r = 25.0 μm; the second with particles of r = 25.0 μm and 14.5 μm; and finally the third, by use of all three types of aluminum oxide particle with r = 25.0, 14.5, and 3.0 μm. To visualize distinctly the individual plots of these measurements on the same graph, the plots of the first two curves were vertically shifted by the same scale interval of 15 but with the same x-axis scale. The right vertical axis shows the fractional volume size distribution (in arbitrary units, percentage not normalized). Comparison between the different peaks of the three size distribution curves shows good correspondence between different measurements on the same sample. On the other hand, the measured size values are in agreement with the corresponding nominal sizes of the calibrated particles in Table 1.

6. Textural Classification

A possibility for the application of these size measurements is represented by the textural classification of soil used in agriculture for characterizing different soil types to optimize their cultivation.

This classification is based on the textural triangle that defines the different soil types dependent on their relative proportions of sand, silt and clay, whose definitions are taken from the standards of the United States Department of Agriculture (USDA).

Table 2. Examples of the Sedimentation Measurements of Quartz Sand[a]

Radius r (μm)	Height h (cm)	Time of Flight $t = h\,(A/r)^2$
$r = 500$	3	$t = 0.067$
	10	$t = 0.223$
	30	$t = 0.67$
$r = 200$	3	$t = 0.42$
	10	$t = 1.39$
	30	$t = 4.2$
$r > 50$	3	$t < 6.68$
	10	$t < 22.3$
	30	$t < 66.8$

[a]Refractive index, (1.55, 0); density, 2648 kg/m^3; $A = 7.4612\ 10^{-4}$ (s m)$^{1/2}$.

The USDA standards[8–11] define the three fundamental soil types on the basis of the mean radius (r) of their particulate as follows:

(1) sand $\quad 50\ \mu\text{m} < r < 2000\ \mu\text{m}$,
(2) silt $\quad 2\ \mu\text{m} < r < 50\ \mu\text{m}$,
(3) clay $\quad r < 2\ \mu\text{m}$.

Since the data elaboration used for our size measurements requires specific parameters (refractive index and density) that depend on the chemical composition of the soil particulate,[12] we had to choose one of the possible soil compositions for each of the three soil types. For this selection, we used the criterion of choosing the most diffuse type of clay (Kaolin clay: $Al_2O_3SiO_22H_2O$), sand, and silt (quartz: SiO_2).

Tables 2–4 present some examples of parameters for performing sedimentation measurements: their evaluation is based on the values for the real and imaginary parts of the refractive index and the density (in kilograms times cubic meter) reported for each of the soil types (sand/silt/clay), with the quantity A (constant for each soil type) defined from Eqs. (8) and (9) as $r = Zt^{-1/2} = A(h/t)^{1/2}$ (with $A = Zh^{-1/2}$). Starting from this constant quantity A, the time of flight, calculated for three h values, is reported for different r values in the last column, in seconds and hours. It is evident from Tables 2–4 that for measuring sand samples ($r > 50\ \mu$m) it is useful to use $h > 5$ cm, whereas for silt and clay ($r < 50\ \mu$m) a suitable value for the height is $h < 5$ cm. For $r < 5\ \mu$m in particular it is better to use $h \approx 3$ cm (measurements to 2 μm, with a duration of the order of 3 h).

Table 3. Examples of the Sedimentation Measurements of Quartz Silt[a]

Radius r (μm)	Height h (cm)	Time of Flight $t = h\,(A/r)^2$
$r = 50$	3	$t = 6.68$ s
	10	$t = 22.3$ s
	30	$t = 66.8$ s
$r = 2$	3	$t = 4175$ s (1.16 h)
	10	$t = 13917$ s (3.87 h)
	30	$t = 41752$ s (11.6 h)

[a]Refractive index, (1.55, 0); density, 2648 kg/m^3; $A = 7.4612\ 10^{-4}$ (s m)$^{1/2}$.

Table 4. Examples of the Sedimentation Measurements of Kaolin Clay[a]

Radius r (μm)	Height h (cm)	Time of Flight $t = h\,(A/r)^2$
$r < 2$	3	$t > 3062$ s (0.85 h)
	10	$t > 10207$ s (2.84 h)
	30	$t > 30622$ s (8.5 h)
$r = 1$	3	$t = 12249$ s (3.4 h)
	10	$t = 40829$ s (11.3 h)
	30	$t = 122487$ s (34 h)

[a]Refractive index, (1.66, 0); density, 3247 kg/m^3; $A = 6.3898\ 10^{-4}$ (s m)$^{1/2}$.

As in the case of aluminum oxide particles, the data elaboration required the values of extinction efficiency Q_{ext}, which were obtained by the Bohren–Huffman–Mie routine[7] for monodispersions centered at each r value considered and by utilizing the refractive index indicated in Tables 2–4. These Q_{ext} values are reported versus the particulate radius in Table 5, where the data corresponding to quartz sand, quartz silt, and kaolin clay are presented in three separate columns. The values of the complex refractive index for quartz and kaolin are indicated in parentheses.

7. Size Distribution and Textural Classification of Soil Samples

Two different soil samples were analyzed by the procedure described above, with the aim of measuring

Table 5. Extinction Efficiency Q_{ext} for Sand/Silt/Clay

r (μm)	Quartz (1.55, 0) Sand	Quartz (1.55, 0) Silt	Kaolin (1.66, 0) Clay
1			2.138
1.5			2.536
2		1.964	1.895
3		1.976	
4		2.431	
5		2.094	
6		1.937	
7		2.208	
8		2.163	
9		1.954	
10		2.098	
20		2.069	
30		2.058	
40		2.051	
50	2.049	2.049	
60	2.042		
70	2.034		
80	2.031		
90	2.025		
100	2.021		
200	2.02		
300	2.02		
400	2.02		
500	2.02		

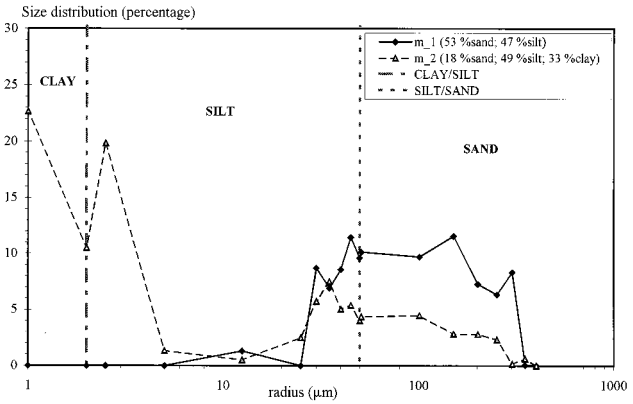

Fig. 4. Fractional volume size distribution of two ground samples.

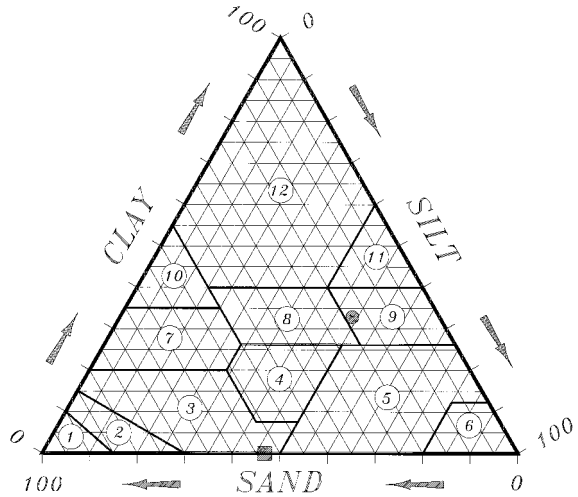

Fig. 5. Textural triangle[8,10]: 1, sand; 2, loamy sand; 3, sandy loam; 4, loam; 5, silt loam; 6, silt; 7, sandy clay loam; 8, clay loam; 9, silty clay loam; 10, sandy clay; 11, silty clay; 12, clay.

their size distribution and then obtaining their textural classification.

Size distribution measurements performed on calibrated aluminum oxide particles were repeated on two ground samples (m-1 and m-2) to be classified. The analysis of experimental data was performed on the basis of the parameters in Tables 2–4 by use of $h = 14$ cm for the first measurement (sample m-1) and $h = 7$ cm for the second one (sample m-2). The fractional volume size distribution was calculated for both samples, and the results are reported in Fig. 4. The size distribution data in Fig. 4 were normalized to have a unitary integral value, and they represent the number of particles (in percentage) having the corresponding radius value.

The classical soil classification of the two ground samples was obtained by measuring their size distributions; however our aim in this paper was to introduce an alternative analysis based on the textural classification. For this purpose, the sand, silt, and clay zones are shown in Fig. 4, where the horizontal axis (radius) is divided into three regions corresponding to sand, silt, and clay for decreasing sizes, as defined in Section 6. Moreover the inset in Fig. 4 shows the textural percentage that was obtained by integrating each sand/silt/clay value separately and normalizing the results to the total integral.

The size distribution curves of Fig. 4 lie mainly in the sand and silt zones for sample m-1, and in the silt and clay zones for sample m-2. This information is summarized by the three values of the textural percentage:

sample m-1	53% sand	47% silt	0% clay
sample m-2	18% sand	49% silt	33% clay

As the final step of the textural classification, the points corresponding to the soil samples must be placed in the textural triangle[8,10] on the basis of the textural percentage values. Sample m-1 has been classified as sandy loam, whereas the results of sample m-2 show it to be silty clay loam. These results are indicated in Fig. 5 by the black marks, a square for m-1 and a circle for m-2.

Starting from the classical soil characterization based on the size distribution in Fig. 4, an alternative classification of soil samples can thus be made using the photosedimentation procedure described in this paper. The textural classification of the two samples is summarized by the points indicated on the reference triangle in Fig. 5 that correspond to the composition of each soil sample.

8. Conclusions

A photosedimentation technique, based on the Stokes formula and the Lambert–Beer law, was used to measure the size distribution of particles in dispersion. Validation and reproducibility of the procedure were proved by measurements on calibrated particulates. Fractional volume size distribution was measured on ground samples from the Tropics (Ghana) and Europe (Italy). The application of this size measurement method can be found in fields such as pharmacology, painting, photography, cement and ceramic powders, and agriculture. In particular, for the selection of a more suitable cultivation, information about soil grain size is essential for classifying ground samples according to the USDA standard of the textural triangle. To make the method applicable in Third World countries, the measurement procedure was developed with the aim of being simple, easy to use, fast, employing low-cost equipment, and as insensitive as possible to operational conditions.

The resulting method is reliable, fast, and easy to realize compared with the traditional hydrometer method that requires laborious ways of analyzing data and longer measurement times.

The authors acknowledge the Third World Academy of Science and the Office of External Activities of the International Centre for Theoretical Physics, Trieste, Italy, for providing funds and equipment for this investigation. We are also grateful to the University of Cape Coast for supporting this research.

References

1. T. Allen, *Particle Size Measurements*, 5th ed., Powder Technical Series, Brian Scarlet, ed. (Chapman & Hall, London, 1997), Secs. 3, 5.5.2, 9.8, 7, 7.8.
2. F. J. Welcher, *Standard Methods of Chemical Analysis*, 6th ed. (Van Nostrand Reinhold, New Jersey, 1995), Vol. 3, Chap. 41.
3. A. C. Groom and J. C. Anderson, "Measurement of size distribution of human erythrocytes by a sedimentation method," J. Cell Physiol. **79,** 127–138 (1971).
4. G. K. Batchelor, "Sedimentation in a dilute dispersion of spheres," J. Fluid Mech. **52,** 245–268 (1972).
5. M. Kerker, *Scattering of Light and Other Electromagnetic Radiation*, E. M. Loebl, ed. (Academic, New York, 1969).
6. M. Born and E. Wolf, *Principles of Optics*, 6th ed. (Pergamon, New York, 1993).
7. C. F. Bohren and D. R. Huffman, *Absorption and Scattering of Light by Small Particles*, (Wiley, New York, 1983).
8. Dirk A. Tel and Myrna Hagarty, eds. *International Institute of Tropical Agriculture* (*ITTA*) *and University of Guelph, Soil and Plant Analyses*. Study guide for agricultural laboratory directors and technologists working in tropical regions, (International Institute for Tropical Agriculture, University of Guelph, Guelph, Canada, 1984).
9. G. Casalicchio and G. Vianello, *Elementi di Pedologia*, (Cooperativa Libraria Universitaria Editrice Bologna, Bologna, Italy, 1979).
10. L. Cavazza, *Fisica del Terreno Agrario*, (Unione Tipografico Editore Torinese, Torino, Italy, 1881).
11. A. J. Koolen and H. N. Kuipers, *Agricultural Soil Mechanics*, (Springer-Verlag, Berlin, 1983).
12. R. C. Weast, ed. *Handbook of Chemistry and Physics*, 52nd ed. (CRC Press, Cleveland, Ohio, 1972).